



Electrocatalysis of Pd–Co supported on carbon black or ball-milled carbon nanotubes towards methanol oxidation in alkaline media

Yi Wang^{a,b}, Xin Wang^a, Chang Ming Li^{a,b,*}

^a School of Chemical and Biomedical Engineering, Nanyang Technological University, 70 Nanyang Drive, Singapore 637457, Singapore

^b Centre for Advanced Bionanosystems, Nanyang Technological University, 70 Nanyang Drive, Singapore 637457, Singapore

ARTICLE INFO

Article history:

Received 8 April 2010

Received in revised form 19 May 2010

Accepted 15 June 2010

Available online 18 June 2010

Keywords:

Pd–Co/C

Methanol oxidation

Fuel cell

Electrocatalysts

Carbon nanotubes

ABSTRACT

Pd/C and Pd–Co/C catalysts were synthesized through a simple simultaneous reduction reaction with sodium borohydride in aqueous solution, and the electrocatalytic performance for methanol oxidation in alkaline solutions was investigated. The structure and morphology of these catalysts were characterized by X-ray diffraction (XRD), energy dispersive X-ray spectroscopy (EDX) and transmission electron microscopy (TEM). The cyclic voltammetry (CV) and CO stripping results show that Pd–Co(8:1)/C has better electrocatalytic activity and higher resistance to CO poisoning over Pd/C, which can be explained by a bifunctional mechanism. Based on the good electrocatalytic performance of Pd–Co(8:1)/C, the ball-milled CNTs-supported Pd–Co(8:1) catalyst was synthesized, demonstrating even better catalytic activity. The high specific surface area of ball-milled CNTs with plenty of mesopores and defects may contribute to the high Pd–Co utilization and consequently to the better electrocatalytic activity.

© 2010 Elsevier B.V. All rights reserved.

1. Introduction

Direct methanol fuel cells (DMFCs) are recognized to be one of the potential power sources for portable electronic devices and electric vehicles [1,2]. A lot of progress has been made in the development of DMFCs [3–5]. However, their performance is still limited by the poor kinetics of the anode reaction [6,7] and the crossover of methanol from the anode to the cathode side through the proton exchange membrane [8,9]. Moreover, high costs of the Pt-based electrocatalysts and susceptibility of the catalysts against poisoning of the CO-like intermediates formed during methanol oxidation (particularly in acidic media) are also the main obstacles to the commercialization of DMFC technology [10]. It is therefore desired to develop low-cost non-platinum electrocatalysts with comparable or improved kinetics for anodic methanol oxidation and better resistance to CO poisoning. Recently, various non-platinum metals have been investigated [10–13]. Among them, Pd is a suitable low-cost transition metal, about 50 times more abundant in earth than Pt [14] and possesses high catalytic activity towards methanol and ethanol oxidation in alkaline media [10,15–18]. Thus, Pd could be a promising anode catalyst in an alkaline DMFC. However, the electroactivity

of Pd for methanol oxidation in alkaline media is needed to be enhanced.

Pt–Co alloy catalysts have been reported [19,20] as both methanol-tolerant cathode and catalytically improved anode for DMFCs. The improvement of methanol oxidation kinetics by selection of Co to modify Pt electrocatalyst is due to lowering the electronic binding energy in Pt through alloying with Co, thus promoting the C–H cleavage reaction at a lower potential. Furthermore, the presence of cobalt oxides provides an oxygen source for CO oxidation at lower potentials. Wang and Xia [21] synthesized PdCo–C catalyst, and found that the catalyst exhibited higher electrocatalytic activity and better stability for formic acid oxidation than that of Pd/carbon catalyst. It was also found that the catalytic activity and stability of Pd₂Co/C for formic acid oxidation were improved by the addition of Co [22]. Pd–Co catalysts also exhibited better electrocatalytic activities for oxygen reduction reaction in acidic media [23,24]. However, to the best of our knowledge, Pd–Co/C bimetallic catalysts for methanol electrooxidation have not been reported yet. In this study, we prepared the Pd/C electrocatalysts containing different amounts of cobalt, and investigated their activity towards the electrooxidation of methanol in alkaline media.

Because of a high aspect ratio and a high specific surface area, carbon nanotubes (CNTs) as a catalyst support to improve the catalyst utilization and electroactivity in fuel cells have been extensively studied [25–27]. Some results have demonstrated that the CNT support induces higher catalytic activity than conventional Vulcan XC-72 carbon black [28,29]. Since the support with a high specific surface area is favorable for metal dispersion, it is of inter-

* Corresponding author at: School of Chemical and Biomedical Engineering, Nanyang Technological University, 70 Nanyang Drive, Singapore 637457, Singapore. Tel.: +65 6790 4485; fax: +65 6791 1761.

E-mail address: ECMLi@ntu.edu.sg (C.M. Li).

est to investigate the suitability of activated CNTs with an increased specific surface area as a support. In our previous work [30], the structure changes of multi-wall carbon nanotubes (MWNTs) after mechanical ball milling were studied. It was found that the specific surface area of a type of short MWNTs with diameter of 5 nm (denoted as S.MWNTs-5) was increased from 472.3 to 823.9 m²/g after 12 h ball-milling treatment. In this paper, based on a good electrocatalytic performance of the Pd–Co/C catalyst, the ball-milled S.MWNTs-5-supported Pd–Co catalyst was synthesized and its catalytic activity was investigated.

2. Experimental

All used chemicals including concentrated ammonia (Sigma–Aldrich), PdCl₂ (Sigma–Aldrich), CoCl₂ (Sigma–Aldrich), NaBH₄ (Sigma–Aldrich), CH₃OH (Sigma–Aldrich), Nafion solution (5% in isopropanol and water), and carbon black (XC-72, Gashub) were analytical grade and used as received. Deionized water was used to prepare samples or solutions.

The raw MWNTs materials were supplied by Shenzhen Nanotech Port Co. Ltd with specifications as described in [30]. In this study, the S.MWNTs-5 (S.MWNTs-5 means short MWNTs with average diameter 5 nm) ball-milled for 12 h were also used as carbon support materials. The specific ball milling process was reported in [30]. The ball-milled MWNTs are denoted as bCNTs.

2.1. Catalyst preparation

To synthesize electrocatalysts, 100 mL aqueous solutions of metal precursors were prepared. After the pH was adjusted to 8–9 using concentrated ammonia, excess amounts of 0.01 M NaBH₄ (freshly prepared) were added dropwise into the solutions. The mixtures were stirred for 2 h. After that, carbon black or bCNTs were added into the mixtures and stirred overnight at room temperature. Then the suspensions were filtered and washed several times with suitable amounts of hot deionized water to completely remove all excess reducing agent. The remaining solids were dried in a vacuum oven for 24 h at ambient temperature. The final catalysts were Pd/C, Pd–Co(8:1)/C, Pd–Co(4:1)/C, Pd–Co(2:1)/C and Pd–Co(8:1)/bCNTs, and the weight percentage of Pd is 15% in these catalysts.

2.2. Catalyst physical characterization method

Structure and morphology of the catalysts were investigated using X-ray diffraction (XRD, Rigaku D/max-2500) and transmission electron microscopy (TEM, JEOL 1400, 120 kV). Elemental analyses were performed using energy dispersive X-ray spectroscopy (EDX, FESEM, JSM-6700F, Japan) measurement. In addition, nitrogen adsorption measurements were performed to characterize the change of the specific surface area and pore volume of carbon support materials.

2.3. Electrochemical experimental procedure

Cyclic voltammetry (CV) and linear sweep voltammetry (LSV) were collected in 1 M KOH + 1 M CH₃OH solution. The working electrode was prepared by dropping 5 μ L of the electrocatalyst ink onto glassy carbon electrode. The ink was prepared by ultrasonically mixing 4 mg of electrocatalyst sample in 2 mL of ethanol. Then, 1 μ L of Nafion solution of 0.5% in 2-propanol was added on top to fix the electrocatalysts. A Pt foil and Hg/HgO (1.0 M KOH) electrode were used as the counter and reference electrodes, respectively. All potentials in the present study were given versus Hg/HgO (1.0 M KOH) electrode. The CV and LSV tests were conducted at 50 and 20 mV/s, respectively, with potential ranging from –0.8 to 0.3 V. The LSV was measured in different temperatures. CO stripping was

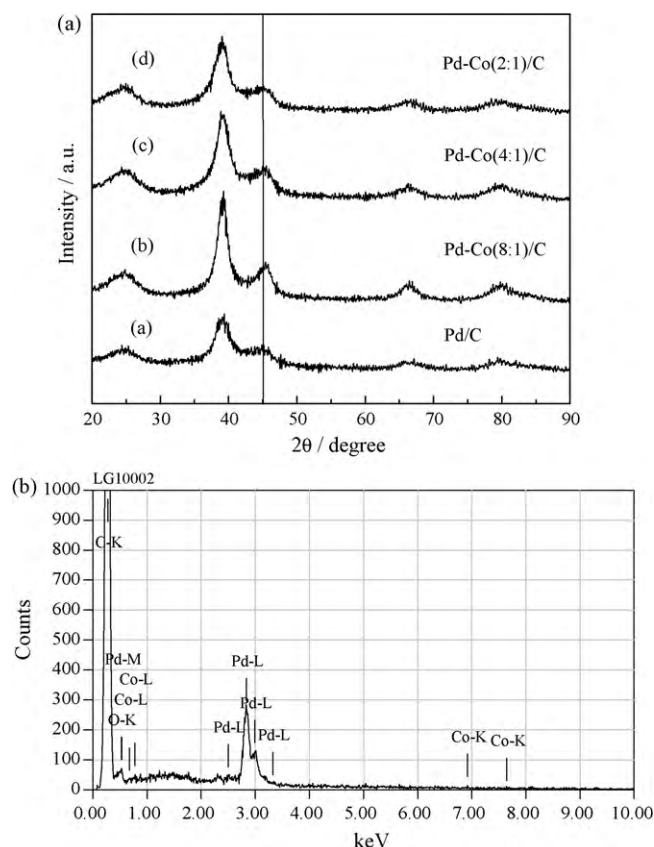


Fig. 1. (a) XRD patterns of the Pd/C, Pd–Co(8:1)/C, Pd–Co(4:1)/C and Pd–Co(2:1)/C catalysts; (b) EDX spectra of the Pd–Co(8:1)/C catalyst.

performed as follows: after purging the solution with N₂ for 20 min, gaseous CO was bubbled for 15 min to form CO adlayer on catalysts while maintaining potential at –0.8 V. Excess CO in solution was purged with N₂ for 20 min and CO stripping voltammetry was recorded in 1.0 M KOH at 50 mV/s.

3. Results and discussion

3.1. Physical characterization and electrocatalytic performance of Pd–Co supported on carbon black

Fig. 1(a) shows the XRD patterns of Pd–Co/C catalysts with different ratios of Pd to Co. For comparison, the XRD pattern of Pd/C is also displayed in Fig. 1(a). The characteristic diffraction peak at about 25° in all the XRD patterns belongs to carbon black support. The main Pd peaks are obvious for each catalyst, but no Co peaks can be seen. However, EDX spectra of the Pd–Co(8:1)/C catalyst clearly show the presence of Co (Fig. 1(b)). This indicates that the Co was either in an amorphous state, or alloyed with the Pd. The diffraction peaks of Pd–Co/C shift a little to higher 2θ value with respect to the corresponding peaks in Pd/C, which indicates that alloying had occurred. However, the extent of the peak shift is small, showing that there is only a little lattice contraction after Co was doped. This may be relative to the fact that the amount of Co is less and some cobalt may be amorphous state. Additionally, a portion of cobalt may be presented in Pd–Co as cobalt oxide, which is much more disposed to amorphization. The crystallite sizes were estimated according to the Scherrer equation $d = 0.9\lambda_{K\alpha 1} / B_{2\theta} \cos \theta_{max}$. The results are 2.8, 3.7, 3.5 and 3.0 nm for the Pd/C, Pd–Co(8:1)/C, Pd–Co(4:1)/C and Pd–Co(2:1)/C catalysts, respectively.

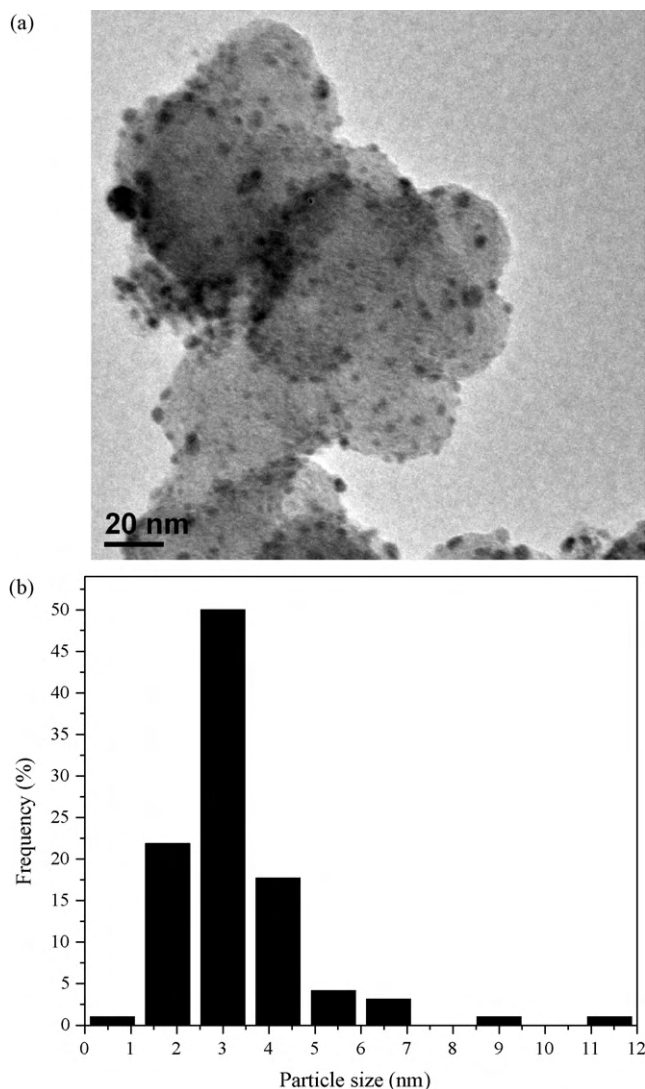


Fig. 2. TEM image (a) and particle size distribution (b) of the Pd–Co(8:1)/C catalyst.

Fig. 2 presents the TEM image and particle size distribution of the Pd–Co(8:1)/C catalyst. It can be observed from Fig. 2(a) that the Pd–Co particles were distributed on the carbon black support. The average particle size seen in the particle size distribution figure was in close proximity to that estimated by XRD.

Fig. 3 displays the cyclic voltammetry on Pd–Co/C and Pd/C electrodes at a scan rate of 50 mV/s in the solution of 1 M CH₃OH and 1 M KOH. The methanol electrooxidation on each electrode of the present investigation has been characterized by two well-defined anodic current peaks: one in the forward (i.e., anodic condition) and the other one in the reverse scan. In the forward scan, the oxidation peak is corresponding to the oxidation of freshly chemisorbed species coming from methanol adsorption. The oxidation peak in the reverse scan is primarily associated with removal of carbonaceous species not completely oxidized in the forward scan than the oxidation of freshly chemisorbed species [31–33]. As seen from Fig. 3, although the onset potentials on these samples are similar, the peak potentials on the Pd–Co/C catalysts are a little more negative than that on the Pd/C catalyst. Moreover, it can be found that the current density on the Pd–Co(8:1)/C catalyst is the highest. However, with the increase of Co content, the current density became lower. For the Pd–Co(2:1)/C catalyst, the current density is obviously lower than that on the Pd/C catalyst. In addition, it can be shown that the ratios of current density of the oxidation peak

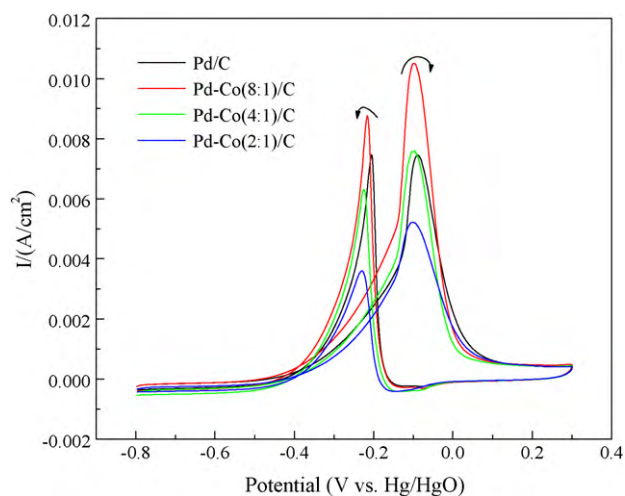


Fig. 3. CVs of methanol electrooxidation on the Pd/C, Pd–Co(8:1)/C, Pd–Co(4:1)/C and Pd–Co(2:1)/C catalysts in 1 M KOH + 1 M CH₃OH solution.

in the forward scan to the oxidation peak in the reverse scan are different among these samples. For Pd/C, the ratio is almost one. After cobalt was added, the ratio increased remarkably. The ratios for Pd–Co(8:1)/C and Pd–Co(4:1)/C are 1.2, and for Pd–Co(2:1)/C, it is 1.4. Usually, the larger the ratio is, the better the performance of the catalyst may be. Because this anodic peak in the reverse scan is attributed to the removal of the incompletely oxidized carbonaceous species formed in the forward scan, and these carbonaceous species are mostly in the form of linearly bonded Pd=C=O [34], the larger ratio of current density of the anodic peak in the forward scan to the anodic peak in the reverse scan may show that the catalyst has a better electrocatalytic activity and resistance to CO poisoning. In sum, according to the CVs (Fig. 3), it is indicated that the Pd–Co(8:1)/C catalyst exhibited the best catalytic activity for methanol oxidation.

To verify if the action of Co in promoting the oxidation is the removal of adsorbed CO by a bifunctional mechanism [35], CO stripping curves were collected, as shown in Fig. 4. It can be found that the onset potential of CO oxidation on the Pd–Co(8:1)/C catalyst was obviously more negative than that on the Pd/C catalyst. This means that the addition of Co facilitated the removal of CO out of the surface of the Pd–Co(8:1)/C. In other words, according to the bifunctional mechanism, the Co activated water at lower potentials than Pd and the activated water could oxidize the adsorbed CO and therefore liberated Pd active sites. This result helped to explain the higher activity of the Pd–Co(8:1)/C for the oxidation of methanol. Fig. 4(b) showed the appearance of two peaks for CO stripping on the Pd–Co(8:1)/C catalyst. Co is not active for CO adsorption. The possible reason for this fact is that some Pd is not alloyed with Co and still remains beside the Pd–Co domain. It indicates the presence of two different surface sites for Pd. One is surface Pd atoms with Co atoms in adjacent sites. As the first peak shows a lower CO stripping potential, it is very likely to be the oxidation by OH species that can be generated in adjacent Co sites at a lower potential. Another surface site is Pd atom without direct contact to Co atoms on the surface, but compared to bulk Pd, the d-band center of these Pd atoms is still affected via the electronic effect from Co oxide, which may lead to the positive shift of peak potential to cause the 2nd peak.

To understand more about the better performance of the Pd–Co(8:1)/C catalyst, LSV tests were performed at several different temperatures on the Pd–Co(8:1)/C and Pd/C electrodes, and the results are shown in Fig. 5. Fig. 6 displays the relationship of the reciprocal of temperature and the logarithm of current density (at

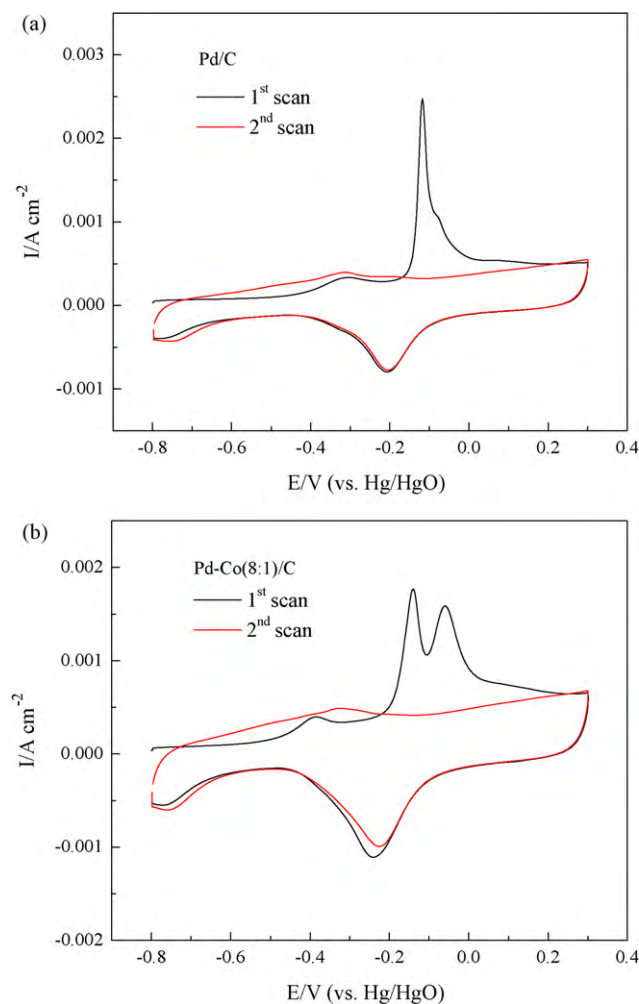


Fig. 4. CO stripping curves on the Pd/C (a) and Pd-Co(8:1)/C (b) catalysts recorded in 1 M KOH solution.

−0.09 V). It was found that the current density on Pd-Co(8:1)/C was always larger than that on Pd/C at all the measuring temperatures. It proves ulteriorly that Pd-Co(8:1)/C has better electrocatalytic performance. Additionally, an apparent activation energy value can be calculated according to Arrhenius equation [36]:

$$I = Ae^{-E_a/RT} \quad (1)$$

where I is the current at a specific potential, R is the gas constant, T is the temperature in K and E_a is the apparent activation energy. By linearly fitting the relationship of $\ln I$ and $1/T$, it can be obtained that the E_a for Pd-Co(8:1)/C and Pd/C is 50.27 and 37.41 kJ/mol, respectively. It is amazing that the E_a became larger after the addition of Co. According to the law of chemical kinetics, the influence of temperature on reaction rate is more prominent for a reaction with a larger apparent activation energy. In other words, if a reaction has a larger E_a , with the increase of temperature, the reaction rate will increase faster. Above a certain temperature, the reaction rate can exceed that of the reaction having a smaller E_a . In this study, although the E_a for Pd-Co(8:1)/C is larger, the reaction rates are faster at all the measuring temperatures. Furthermore, the measuring temperatures just fall in the range of operating temperature of DMFCs. Thus, the electrocatalytic performance of the Pd-Co(8:1)/C catalyst is still promising.

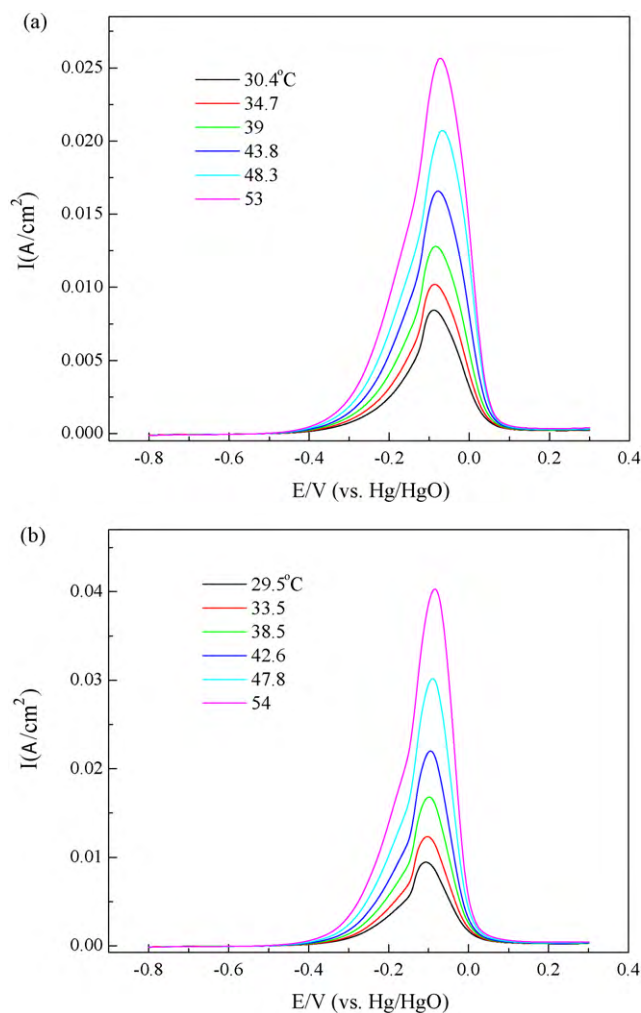


Fig. 5. LSV curves in 1 M KOH + 1 M CH₃OH solution at different temperatures for (a) Pd/C and (b) Pd-Co(8:1)/C, scan rate: 20 mV/s.

3.2. Physical characterization and electrocatalytic performance of Pd-Co supported on ball-milled CNTs

Based on the good electrocatalytic performance of the Pd-Co(8:1)/C catalyst, the ball-milled S.MWNTs-5-supported

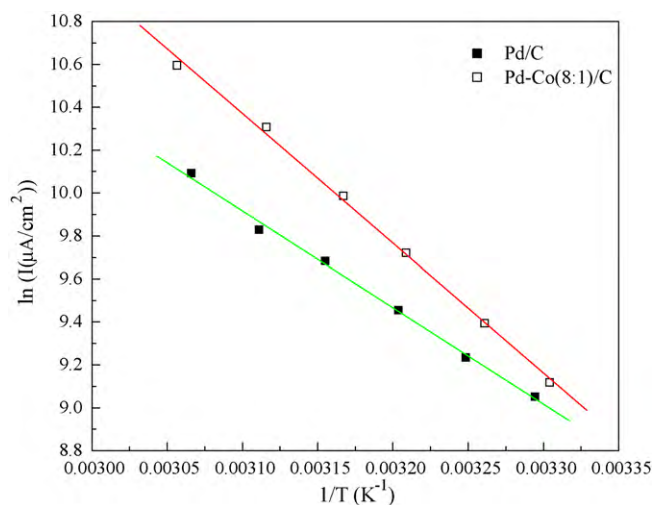


Fig. 6. The plot of $\ln I$ vs. $1/T$ (I : current density at −0.09 V; T : temperature in K).

Table 1

Pore structure of the carbon black, pristine and ball-milled CNTs.

Sample	Total specific surface area, S_{BET} (m^2/g)	Total pore volume (cm^3/g)	Micropore volume (cm^3/g)	Mesopore volume (cm^3/g)
Carbon black	254.4	0.3409	0.1212	0.2197
Pristine CNTs	472.3	1.083	0.1604	0.9226
Ball-milled CNTs	823.9	1.807	0.2556	1.5514

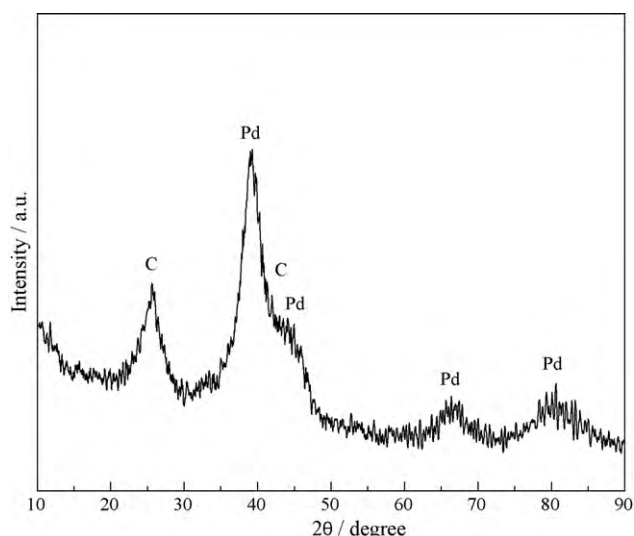
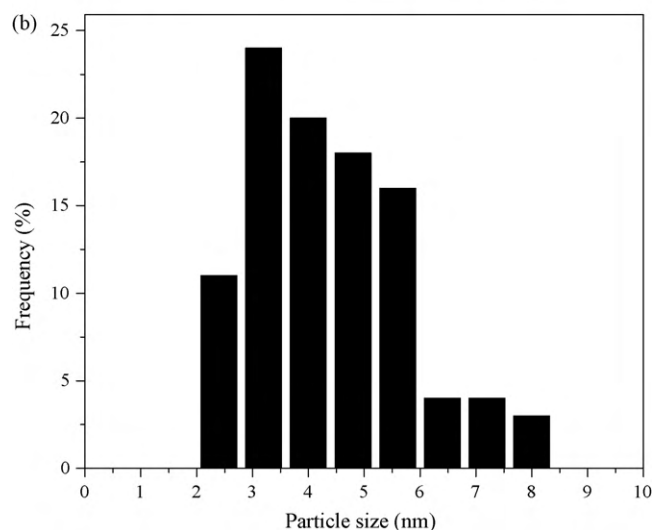
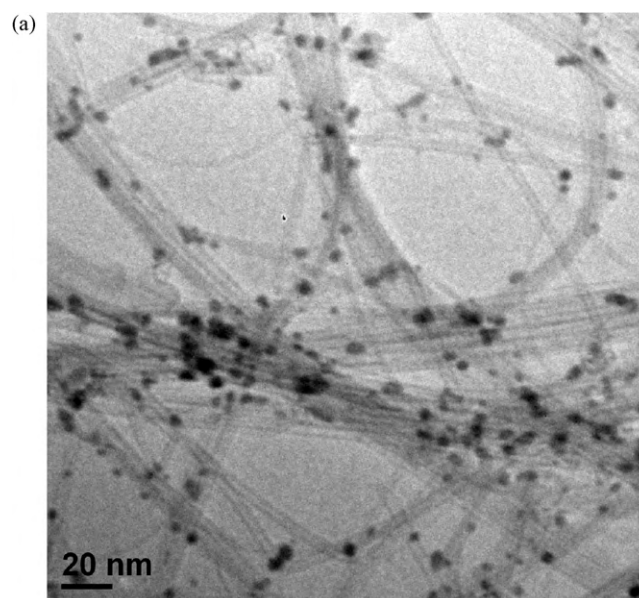
Pd–Co(8:1) catalyst was synthesized and its catalytic activity was investigated. According to our previous work [30], after ball-milling, the CNTs were shortened and open-ended, and the defects were increased. Typical pore structure of carbon black, pristine and ball-milled CNTs analyzed via BET equation is presented in Table 1. As can be seen from the table, the total S_{BET} and pore volume of bCNTs reach $823.9 \text{ m}^2/\text{g}$ and $1.807 \text{ cm}^3/\text{g}$, respectively. These values are about 3.2 and 5.3 times larger than the values of carbon black ($254.4 \text{ m}^2/\text{g}$ and $0.3409 \text{ cm}^3/\text{g}$), respectively. In particular, the volume of mesopores was remarkably increased, which indicates that the bCNTs possessed a large amount of mesopores. It is very important for the Pd–Co deposition with small size and uniform distribution.

The XRD pattern of the Pd–Co(8:1)/bCNTs catalyst is shown in Fig. 7. The peak at about 26° which belongs to the graphitic plane is clearly observed. Combined with the TEM images in the literature [30], it is indicated that the crystalline structure of CNTs was basically maintained after ball-milling treatment. In addition, a few strong peaks of palladium are also clearly observed. According to the Scherrer equation, the crystallite size of Pd was estimated to be 2.8 nm.

Fig. 8 presents the TEM image and particle size distribution of the Pd–Co(8:1)/bCNTs catalyst. The fine Pd–Co nanoparticles are distributed on the surface of bCNTs. Moreover, it can be found that the aggregating extent of the Pd–Co nanoparticles was very low.

The CVs of Pd–Co(8:1)/bCNTs in $\text{CH}_3\text{OH}/\text{KOH}$ solution are shown in Fig. 9. For comparison, the CVs of Pd–Co(8:1)/C are also shown in this figure. As compared with Pd–Co(8:1)/C, the current density on Pd–Co(8:1)/bCNTs is obviously higher. It shows that the Pd–Co(8:1)/bCNTs catalyst has a better catalytic activity. Furthermore, for the catalyst supported on bCNTs, the ratio of current density of the oxidation peak in the forward scan to the oxidation peak in the reverse scan reaches 1.4, which is even higher than that of Pd–Co(8:1)/C. Fig. 10 shows CO stripping curves on the Pd–Co(8:1)/bCNTs catalyst. It can be found that the onset poten-

tial of CO oxidation on the Pd–Co(8:1)/bCNTs catalyst is similar to that on the Pd–Co(8:1)/C catalyst. It indicates that the resistance to CO poisoning of Pd–Co(8:1)/bCNTs is also good. Therefore, the Pd–Co(8:1) catalyst supported on bCNTs could be a more promising catalyst for methanol oxidation in alkaline media. It may need to be point out that Pd–Co has been reported being a good catalyst for oxygen reduction and tolerant to methanol [23]. In terms of our experimental results, this may only indicate Pd–Co can be a catalyst for both oxygen reduction and methanol oxidation, but the former is favored over the latter. In addition, the surface properties of the catalyst in two cases are actually different. The former was conducted in acidic environment, thus resulting in leaching out of the surface Co species while leaving rough Pd

**Fig. 7.** XRD pattern of the Pd–Co(8:1)/bCNTs.**Fig. 8.** TEM image (a) and particle size distribution (b) of the Pd–Co(8:1)/bCNTs.

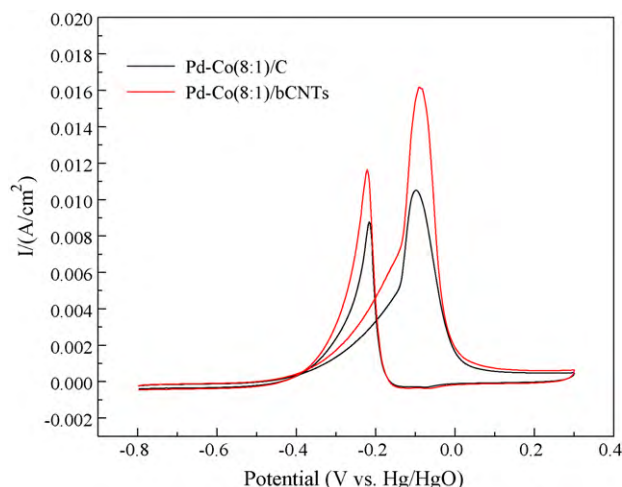


Fig. 9. CVs of methanol electrooxidation on the Pd–Co(8:1)/C and Pd–Co(8:1)/bCNTs catalysts in 1 M KOH + 1 M CH₃OH solution.

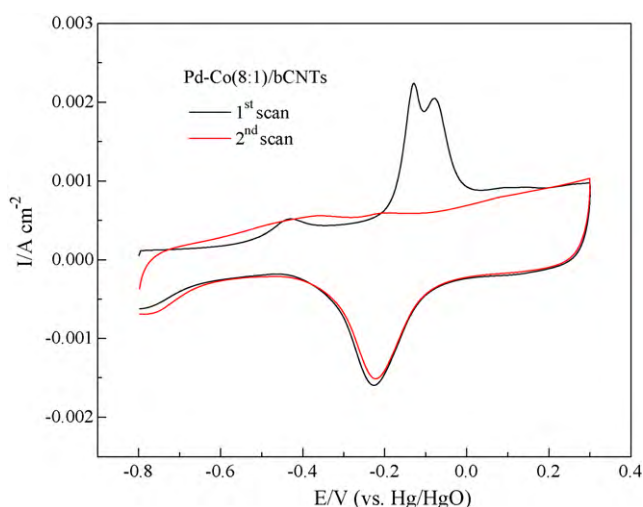


Fig. 10. CO stripping curves on the Pd–Co(8:1)/bCNTs catalyst recorded in 1 M KOH solution.

skin layer with underlying alloy structure. In this work, Co species in alkaline environment can remain intact on the surface to provide oxygen containing species for methanol oxidation at a lower potential.

It is well known that small size of Pd particles with uniform distribution will improve the electrochemical activity. The support materials having scales of mesopores will be in favor of Pd deposition. The present bCNTs contain plenty of micro-/mesopores especially mesopores and thus possess a very high S_{BET} . As a result, the bCNTs displayed a better Pd–Co-loading dispersion, which was more uniform and had a lower aggregating extent, and thus improved the Pd–Co utility ratio and electrochemical properties. This may result in the better electrocatalytic performance of the Pd–Co(8:1)/bCNTs catalyst.

4. Conclusions

The Pd–Co/C catalysts with different amounts of cobalt were prepared, and the catalytic performance towards methanol electrooxidation in alkaline media was investigated. As compared with the Pd/C catalyst, the Pd–Co(8:1)/C catalyst has better electrocatalytic activity and higher resistance to CO poisoning, which can be explained by a bifunctional mechanism. Although the apparent activation energy is increased after the addition of cobalt, the current density was still higher in the range of operating temperature of DMFCs. Based on the good electrocatalytic performance of the Pd–Co(8:1)/C, the ball-milled CNTs-supported Pd–Co(8:1) catalyst was synthesized, and it exhibited better catalytic activity. The high S_{BET} of bCNTs with plenty of mesopores and defects may contribute to the high Pd–Co utility and consequently to the better electrochemical activity.

Acknowledgements

The authors are grateful to the financial support by Center of Advanced Bionanosystems in Nanyang Technological University.

References

- [1] M.A. Scibioh, S.K. Kim, E.A. Cho, T.H. Lim, S.A. Hong, H.Y. Ha, *Appl. Catal. B* 84 (2008) 773.
- [2] M.A. Scibioh, I.H. Oh, T.H. Lim, S.A. Hong, H.Y. Ha, *Appl. Catal. B* 77 (2008) 373.
- [3] N.Y. Hsu, C.C. Chien, K.T. Jeng, *Appl. Catal. B* 84 (2008) 196.
- [4] J.H. Kim, B. Fang, S.B. Yoon, J.S. Yu, *Appl. Catal. B* 88 (2009) 368.
- [5] C.S. Chen, F.M. Pan, *Appl. Catal. B* 91 (2009) 663.
- [6] T.D. Jarvi, S. Sriramulu, E.M. Stuve, *J. Phys. Chem. B* 101 (1997) 3646.
- [7] E. Reddington, A. Sapienza, B. Gurau, R. Viswanathan, S. Sarangapani, E.S. Smotkin, T.E. Mallouk, *Science* 280 (1998) 1735.
- [8] A. Heinzel, V.M. Barragán, *J. Power Sources* 84 (1999) 70.
- [9] K. Ramya, K.S. Dhathathreyan, *J. Electroanal. Chem.* 542 (2003) 109.
- [10] Z.L. Liu, X.H. Zhang, L. Hong, *Electrochem. Commun.* 11 (2009) 925.
- [11] M. Jafarian, R.B. Moghaddam, H. Heli, F. Gopal, H. Khajehsharifi, M.H. Hamed, *Electrochim. Acta* 48 (2003) 3423.
- [12] A. Serov, C. Kwak, *Appl. Catal. B* 90 (2009) 313.
- [13] H. Heli, M. Jafarian, M.G. Mahajani, F. Gopal, *Electrochim. Acta* 49 (2004) 4999.
- [14] O. Savadogo, K. Lee, K. Oishi, S. Mitsushima, N. Kamiya, K.-I. Ota, *Electrochem. Commun.* 6 (2004) 105.
- [15] P.K. Shen, C.W. Xu, *Electrochem. Commun.* 8 (2006) 184.
- [16] C. Xu, H. Wang, P.K. Shen, S.P. Jiang, *Adv. Mater.* 19 (2007) 4256.
- [17] S.T. Nguyen, H.M. Law, H.T. Nguyen, N. Kristian, S. Wang, S.H. Chan, X. Wang, *Appl. Catal. B* 91 (2009) 507.
- [18] R.N. Singh, A. Singh, Anindita, *J. Solid State Electrochem.* 13 (2009) 1259.
- [19] E. Antolini, J.R.C. Salgado, E.R. Gonzalez, *Appl. Catal. B* 63 (2006) 137.
- [20] H.B. Zhao, J. Yang, L. Li, H. Li, J.L. Wang, Y.M. Zhang, *Int. J. Hydrogen Energy* 34 (2009) 3908.
- [21] X.M. Wang, Y.Y. Xia, *Electrochem. Commun.* 10 (2008) 1644.
- [22] R.F. Wang, S.J. Liao, S. Ji, *J. Power Sources* 180 (2008) 205.
- [23] X. Li, Q. Huang, Z. Zou, B. Xia, H. Yang, *Electrochim. Acta* 53 (2008) 6662.
- [24] W. Wang, D. Zheng, C. Du, Z. Zou, X. Zhang, B. Xia, H. Yang, D.L. Akins, *J. Power Sources* 167 (2007) 243.
- [25] J. Prabhuram, T.S. Zhao, C.W. Wong, J.W. Guo, *J. Power Sources* 134 (2004) 1.
- [26] C. Zhou, S. Kumar, C.D. Doyel, J.M. Tour, *Chem. Mater.* 17 (2005) 1997.
- [27] J.J. Niu, J.N. Wang, *Electrochim. Acta* 53 (2008) 8058.
- [28] H. Shi, *Electrochim. Acta* 41 (1996) 1633.
- [29] S.C. Roy, P.A. Christensen, A. Hamnett, K.M. Thomas, V. Trapp, *J. Electrochem. Soc.* 143 (1996) 3073.
- [30] Y. Wang, W.Q. Deng, X.W. Liu, X. Wang, *Int. J. Hydrogen Energy* 34 (2009) 1437.
- [31] J.C. Huang, Z.L. Liu, C.B. He, L.M. Gan, *J. Phys. Chem. B* 109 (2005) 16644.
- [32] J. Liu, J. Ye, C. Xu, S.P. Jiang, Y. Tong, *Electrochem. Commun.* 9 (2007) 2334.
- [33] M.W. Xu, G.Y. Gao, W.J. Zhou, K.F. Zhang, H.L. Li, *J. Power Sources* 175 (2008) 217.
- [34] R. Manohara, J.B. Goodenough, *J. Mater. Chem.* 2 (1992) 875.
- [35] J.M. Leger, S. Rousseau, C. Coutanceau, F. Hahn, C. Lamy, *Electrochim. Acta* 50 (2005) 5118.
- [36] J.L. Cohen, D.J. Volpe, H.D. Abruna, *Phys. Chem. Chem. Phys.* 9 (2007) 49.